High energy and high peak power GHz burst-mode all-fiber laser with uniform envelope and tunable intra-burst pulses

Shuailin Liu[1,2,3], Bin Zhang[1,2,3], Yuanzhuang Bu[1,2,3], Desheng Zhao[1,2,3], Xiran Zhu[1,2,3], Linyong Yang[1,2,3] and Jing Hou[1,2,3]

[1] *College of Advanced Interdisciplinary Studies, National University of Defense Technology, Changsha 410073, China*

[2] *Nanhu Laser Laboratory, National University of Defense Technology, Changsha 410073, China*

[3] *Hunan Provincial Key Laboratory of High Energy Laser Technology, Changsha 410073, China*

Abstract

We report a Yb-doped all-fiber laser system generating burst-mode pulses with high energy and high peak power at GHz intra-burst repetition rate. To acquire the uniform burst envelope, a double-pre-compensation structure with an arbitrary waveform laser diode driver and an AOM is utilized for the first time. The synchronous pumping is utilized to the system to reduce the burst repetition rate to 100 Hz and suppress the amplified spontaneous emission (ASE) effect. By adjusting gain of every stage, the uniform envelopes with different output energies can be easily obtained. The intra-burst repetition rate can be tuned from 0.5 to 10 GHz actively modulated by an electro-optic modulator. Optimized by timing control of 8 channels of analog signal and amplified by 7 stages of Yb-doped fiber amplifier,

This peer-reviewed article has been accepted for publication but not yet copyedited or typeset, and so may be subject to change during the production process. The article is considered published and may be cited using its DOI.

10.1017/hpl.2023.62

the pulse energy achieves 13.3 mJ at 0.5 ns intra-burst pulse duration, and the maximum peak power reaches ~3.6 MW at 48 ps intra-burst pulse duration. To the best of our knowledge, for reported burst-mode all-fiber lasers, this is the output energy and peak power records with nanosecond level burst duration, and the widest tuning range of intra-burst repetition rate. In particular, this flexibly tunable burst-mode laser system can be directly applied to generate high power frequency-tunable microwave.

Key words: high pulse energy, high peak power, burst-mode laser, fiber laser

Correspondence to: College of Advanced Interdisciplinary Studies, National University of Defense Technology, Changsha 410073, China. Email: nudtzhb@163.com (Bin Zhang) and houjing25@sina.com (Jing Hou)

I. Introduction

Burst-mode lasers generate a string of closely spaced short pulses in a lower repetition, achieving high repetition rate and high peak power simultaneously. Some applications of high energy and high peak power burst-mode lasers include materials procession [1-6], precision surgery [7-9], high resolution detection [10-12], high power microwave generation [13] and so on. A novel application in recent years for burst-mode laser is high power pulsed agile microwave generation. A few studies have been reported on a pulsed laser illuminating a photoconductive semiconductor switch (PCSS) to generate narrowband microwave which possesses the identical waveform of the laser pulses [14-16]. The frequency spectrum and peak power of the microwave depend on that of the laser pulse. Particularly, the laser working in burst-mode is beneficial to

https://doi.org/10.1017/hpl.2023.62 Published online by Cambridge University Press

generate high frequency (over GHz-level), high power, and agile frequency microwave burst signal, for which some output characteristics need to be considered. For one thing, the evenly distribution of the burst envelope affects the effective microwave burst duration. For another, the intra-burst repetition rate needs to be tuned flexibly to yield frequency-adjustable microwave signal. Therefore, approximate uniform envelope and tunable frequency for burst-mode laser are required.

In 2021, we have demonstrated that, for the first time, an uniform envelope burst-mode fiber laser system is employed to generate narrowband microwave with tunable frequency (0.80-1.12 GHz) by illuminating a linear-state PCSS [13]. To compensate for the envelope distortion caused by the gain saturation effect, the pre-compensation envelope shaping according to the inverse Frantz-Nodvik-equation [17, 18] is realized. The pulse energy and peak power of laser is 200 μJ and 4 kW respectively, and the generated microwave power is 300 W. However, if the laser peak power were further promoted for higher microwave power output, the envelope would suffer more severe waveform distortion due to the larger gain of the front edge. In the same year, a 4 mJ burst-mode laser system is constructed based on a fiber-solid hybrid structure, whose burst repetition rate is reduced to 100 Hz and peak power reaches 80 kW [19]. On the one hand, the free-space configuration for solid-state laser amplifier occupies enormous space and is inconvenient for practical application. On the other hand, the reliability and stability of solid laser amplifiers are inferior to that of fiber laser amplifiers. Therefore, the all-fiber structure and a new scheme for the higher power pulse pre-compensation become the development directions of the burst-mode laser for high power microwave generation.

Moreover, to adapt for other different application requirements, in addition to increasing the burst energy and peak power, it is necessary to promote tuning performance of burst mode

https://doi.org/10.1017/hpl.2023.62 Published online by Cambridge University Press

laser in time domain, including repetition rate and duration of intra-burst pulse. As we know, there are four implementation constructions the reported high energy/high peak power burst-mode fiber lasers. The first way is to employ a mode-locked fiber laser modulated by an acoustic optical modulators (AOM) periodically cutting off pulse train [20, 21]. The second way is to utilize the pulse fiber multiplier to achieve high repetition rate of intra-burst pulse [22-24]. However, these two methods are unable to flexibly adjust repetition rate of intra-burst pulse. Direct seed shaping technology is convenient generate arbitrarily tunable burst-mode pulse, which is the third way [25], but limited by circuit performance, this method could only generate intra-burst pulse at μs-ns level. The fourth way is to use electro-optical modulator (EOM) to modulate at a very fast rate [13, 26], which could achieve the widest tuning range of ps-ns pulse duration and over GHz repetition rate in theory. However, because of high insertion loss and the single-mode fiber input, it is difficult to amplify the weak signals from EOM while maintaining the uniformity of envelope. There is no report to realize such high energy burst-mode fiber laser.

In this report, we demonstrate a high pulse energy and high peak power all-fiber burst-mode laser system whose repetition rate and duration of intra-burst pulse is tunable. To achieve the burst envelope approximately uniform in seven stages of fiber amplifier, we promote a new scheme for pre-compensation combining an arbitrary waveform laser diode driver and an AOM, which is called double-pre-compensation structure. The laser system can deliver burst-mode pulses with frequency of 0.5-10 GHz tunable and intra-burst pulse duration of 48 ps-0.5 ns tunable. Meanwhile, we construct a multiplex synchronous timing system to realize the synchronous pumping for every stage of amplifier. At the main amplifier, a 100 μm core diameter gain fiber is utilized to acquire the higher energy and reduce the nonlinear effect, so the highest energy of 13.3

https://doi.org/10.1017/hpl.2023.62 Published online by Cambridge University Press

mJ and the highest peak power of ~3.6 MW for burst-mode pulse is achieved. This laser system is useful for the high power microwave generation and other potential applications.

II. Experimental setup

A schematic diagram of the laser system setup is depicted in Fig. 1(a). The laser system is mainly segmented into 5 parts: a pulsed seed, three stages of single mode pre-amplifier, a high repetition rate modulation part, a secondary pre-compensation modulation part, and four stages of multimode amplifier. The seed laser is a 1064 nm Fabry-Perot (FP) laser diode (LD) with peak power of 1 W and 3 dB bandwidth of ~2 nm. One arbitrary waveform LD driver is utilized to directly modulate the seed LD into the pre-compensated waveform with the repetition rate of 100 Hz.

There are three stages for the single mode pre-amplifiers, whose gain mediums are all highly doped single mode Yb^{3+}-doped fibers (YDFs) with the absorption coefficient of 250 dB/m at 976 nm and pump sources are single mode 976 nm LDs. The high repetition rate modulation part includes an EOM with bandwidth of 10 GHz and an arbitrary waveform generator (AWG-1, Keysight M8195A) generating high speed electric signal with 45 GHz bandwidth. The secondary pre-compensation modulation part includes an AOM with bandwidth of 200 MHz and an AWG-2 exporting pre-compensation waveform. The AOM not only reforms the pulse shape to the pre-compensation waveform, but also blocks the amplified ASE pedestal from the pre-amplifiers in the time domain. It is worth noting that the third stage of single mode pre-amplifier is positioned after the EOM and before the AOM. This stage of amplifier makes up the insertion loss and modulation of the EOM and provides the relatively high initial energy for the secondary pre-compensation of the AOM. An isolator/bandpass filter (IBP) with the 3 dB bandwidth of 2 nm is placed after the AOM. The multi-mode amplifiers in the system consist of four all-fiber double-

https://doi.org/10.1017/hpl.2023.62 Published online by Cambridge University Press

clad amplifier stages, which are shown as the 4th to 7th amplifiers in Fig. 1. The 4th amplifier employs a 3 m 15/130 μm double-clad YDF (DCYDF) with the absorption coefficient of 5.4 dB/m at 976 nm, and an isolator (ISO) is employed to avoid the backward reflections of the following amplifiers. The 5th amplifier uses a 2.5 m 30/250 μm DCYDF with the absorption coefficient of 7.5 dB/m at 976 nm. The 6th amplifier uses a 2.8 m 48/400 μm DCYDF with the absorption coefficient of 7.5 dB/m at 976 nm. The main amplifier employs a 1.8 m 100/400 μm DCYDF with the absorption coefficient of 22.5 dB/m at 976 nm. Moreover, a 400 μm coreless fiber is spliced as the end cap at the end of the main amplifier to avoid damage of the output end face.

In order to realize synchronous pumping and the secondary pre-compensation technique, a multiplex synchronous timing system is employed to the seed, AOM and every stage of amplifier in the laser system [27]. There is rather low repetition rate (100 Hz) for signal and pump pulse so that the system operates in a relatively low average power level. Therefore, the amplifiers are free of cooling, and the volume required for the whole system is greatly compressed. The time sequence of seed and pump pulses is illustrated in Fig. 1(b). Considering the burst energy, fiber parameters and the peak power pump LDs could supply, the pump energy and width in every stage are optimized in experiment to suppress ASE and nonlinear effect. The seed pulse arrives at the end of the pump pulse, so that the stored particle in the upper level by pumping is consumed, and the extraction of stored energy by ASE is reduced. It should be noticed that the last two stages of pump energies need to adjust for the tunable output parameters.

The green waveforms and arrows in Fig. 1(a) depict the waveform evolution of 100 Hz laser pulse from seed to output. Firstly, a pre-compensation pulse waveform is loaded to the LD seed driver. Secondly, two stages of pre-amplifier promote the pulse energy and bring about the waveform distortion at the same time. Thirdly, GHz modulation is loaded to pulses by the EOM

https://doi.org/10.1017/hpl.2023.62 Published online by Cambridge University Press

and the pulses are modulated into burst-mode pulses. After the third stage of pre-amplifier, the AOM shapes the burst, which presents distortion of low front and high back caused by gain saturation effect from the pre-amplifiers to the pre-compensation waveform. Finally, four stages of multi-mode amplifier boost the pulse energy to ~mJ level and the output burst waveform distributed approximately uniformly.

The temporal laser pulse train and radiofrequency (RF) spectrum is monitored by a 36 GHz high-speed digital oscilloscope (Lecroy, LM-10-35-ZI), connected with a 45 GHz InGaAs photodetector. The optical spectrum is detected by an optical spectrum analyzer (YOKOGAWA, AQ6370). Two pyroelectric energy meters (Ophir PE9-ES-C and PE50-DIF-C) are employed to detect relatively low (<100 μJ) and high (>100 μJ) pulse energy, respectively.

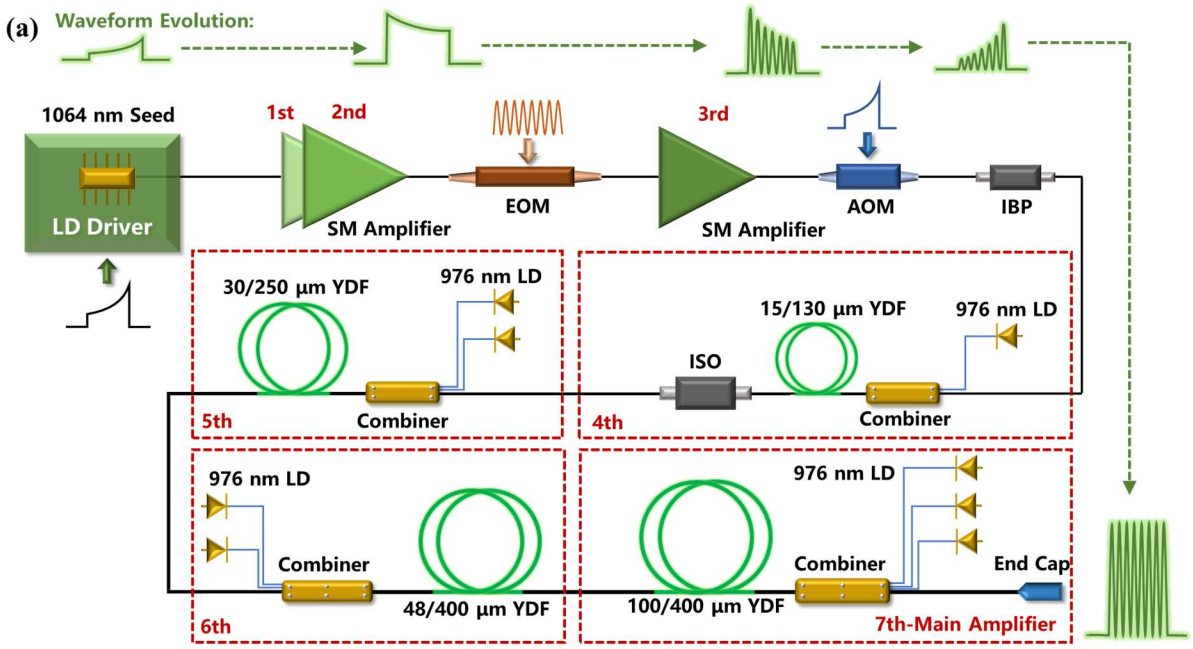

https://doi.org/10.1017/hpl.2023.62 Published online by Cambridge University Press

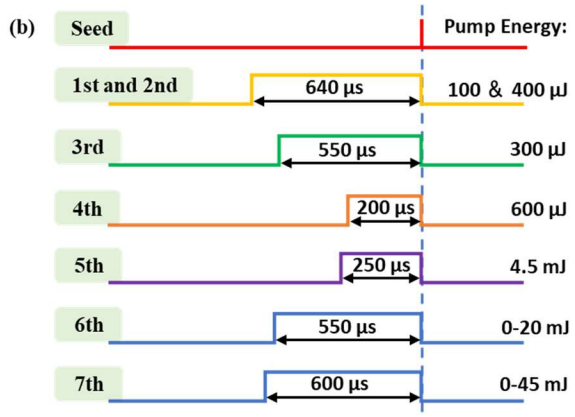

Fig.1. (a) The schematic diagram of the laser system. LD: laser diode, IWDM: isolator/wavelength division multiplexer hybrid, IBP: isolator/bandpass filter hybrid, SM: single mode, YDF: wavelength division multiplex, AOM: acousto-optic modulator, ISO: isolator; (b) Time sequence of seed and pump pulses.

III. Results and discussion

In the experiment, the laser system is investigated in detail firstly at 1 GHz repetition rate and 50% intra-burst duty cycle. As for seed, to make it more convenient for seed pulse amplification and leave leeway for the secondary pre-compensation, the seed pulse duration is longer than that of the output burst, which is set to ~70 ns. The laser system is divided into two parts, the first three single-mode amplifiers and the last four multi-mode amplifiers, to calculate the pre-compensation. According to the inverse Frantz-Nodvik-equation, two pre-compensation waveforms are calculated as shown in Fig. 2. The electrical signal waveform for seed driver (blue line) and the pulse train of seed (red line) are depicted in Fig. 2(a). A pre-compensated envelope for seed is loaded to the LD seed driver. The pulse duration of seed is ~70 ns, which is longer than the waveform because of ascending and descending time for electrical modulation. Blue line and red line in Fig. 2(b) illustrate the pre-compensation waveform from AWG signal and the burst-mode pulse waveform after AOM modulation, respectively. The envelope of burst-mode pulse generally resembles the pre-compensated waveform. Here, we obtain the pre-compensated burst-mode seed with burst duration of ~60 ns.

https://doi.org/10.1017/hpl.2023.62 Published online by Cambridge University Press

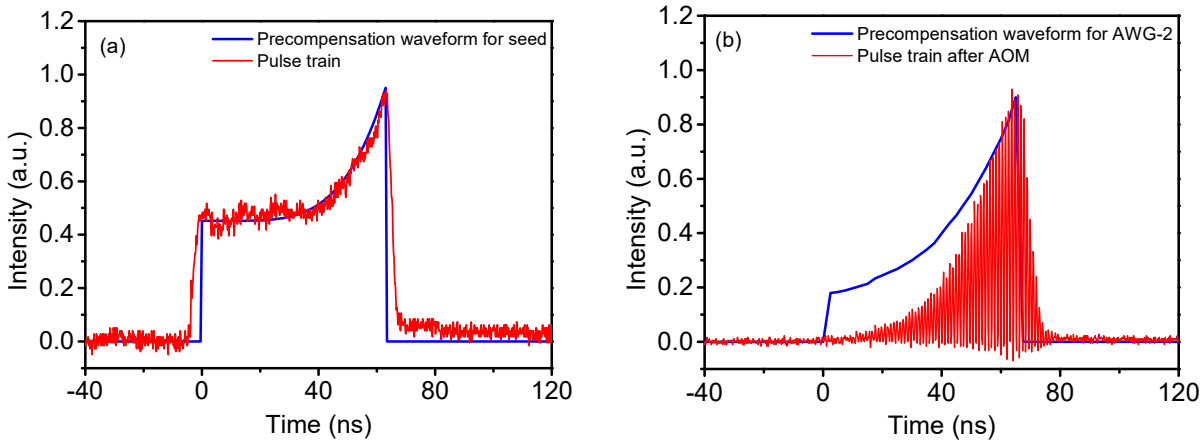

Fig. 2. Evolution of the pulse shape during the secondary pre-compensation process. (a) The signal waveform for seed driver and the pulse train of seed; (b) The signal waveform from AWG and the burst-mode pulse waveform after AOM modulation.

The burst-mode seed is introduced into four stages of multimode amplifier to enhance the pulse energy. Figure 3(a) shows the pulse energy changing with the pump energy of the main amplifier, which manifests the slope efficiency of 46.96%. The maximum pulse energy achieves 13.3 mJ, which is the highest energy for all-fiber GHz burst-mode pulse to our knowledge, and the calculated highest peak power reaches ~0.53 MW. The extraction efficiency is 31.4% at the maximum energy. The temporal shape evolution of the burst-mode pulse after the main amplifier is shown in Fig. 3(b). The front part of burst envelope lifts with the pump power increasing on account of gain saturation effect, and the approximately uniform envelope is achieved at the maximum output energy, which indicates that the gain saturation effect is mitigated successfully by secondary pre-compensation. Because of the relatively slow rising and falling time of AOM modulation (~10 ns), it is unable to achieve rapid edge for both sides of envelope. Figure 3(c) depicts the local intra-burst pulse and the setup signal in detail, showing a stable format for the intra-burst pulse. The amplified intra-burst pulse stays ~0.5 ns. As shown in Fig. 3(d), the spectrum of the output laser broadens gradually with the increase of pulse energy mostly resulting from self-phase modulation. At the maximum output energy, 3 dB and 20 dB bandwidth are respectively 7.8

https://doi.org/10.1017/hpl.2023.62 Published online by Cambridge University Press

nm and 42.6 nm. However, the ASE component gradually grows at 1.03 μm band when the energy increases over ~3 mJ and the intensity difference of the signal peak and ASE spectrum is ~30 dB at the maximum energy. If the pump energy is further increased, it would occur self-stimulation effect which could damage the laser system. Therefore, the enhancement of burst-mode pulse energy is mainly limited by ASE.

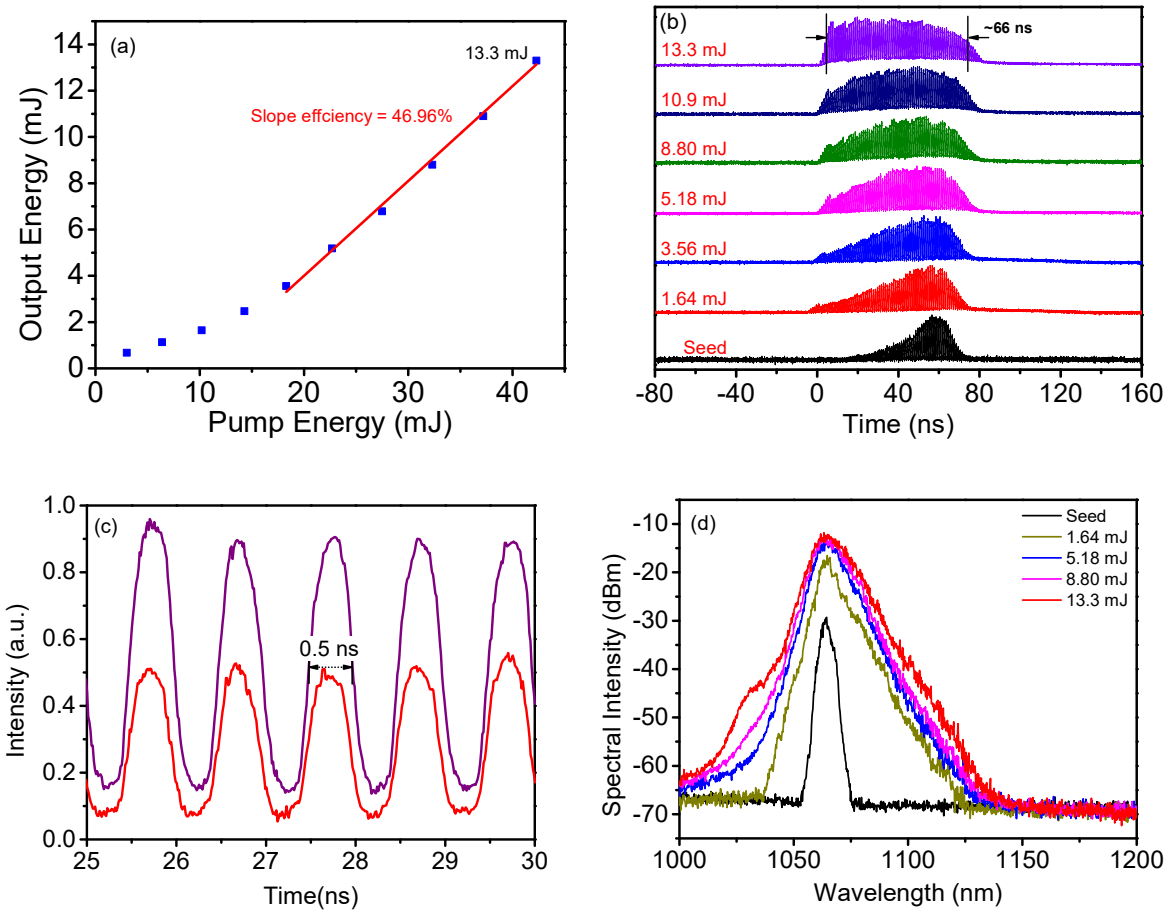

Fig. 3. Performance of the output burst-mode laser. (a) Variation of pulse energy with different pump energy of the main amplifier; (b) Temporal shape of the pulse with different pulse energy; (c) Comparison of intra-burst pulse in detail between seed and output; (d) Spectrum evolution of the seed and main amplifier.

We have noticed that there is different degree of waveform distortion to the burst-mode pulse for each amplifier because of variant gain saturation effect brought by different types of YDF. Therefore, the burst envelope can keep approximately uniform in different pulse energy by

https://doi.org/10.1017/hpl.2023.62 Published online by Cambridge University Press

adjusting pump power of each stage of amplifier. To study the uniformity of the burst envelope, we define an envelope uniformity factor as a relative standard deviation (RSD) of the peak power in a burst, which is presented as

$$U = \frac{1}{P_{Avg}} \sqrt{\frac{\sum_{i=1}^{n} (P_i - P_{Avg})^2}{n}} \times 100\% \quad (1)$$

where U represents the uniformity factor; n is the intra-burst pulse number in the calculation region of a burst; P_i and P_{Avg} are peak power of every intra-burst pulse and the average peak power, respectively. It is worth noting that the bandwidth limitation of the AOM leads to ~10 ns rising and falling time of AOM modulation. As shown in the inset of Fig. 4, the rising edge of burst is 10 ns period from the beginning of modulation signal (T_1), and the falling edge of burst is the optical modulation time after the end of the AWG signal (T_3), which are both excluded from calculation. In other words, the calculation region of envelope uniformity factor is from the moment 10 ns after the start of the modulation signal to the moment when the modulation signal ends (T_2). The burst-mode pulse can be regarded as relatively uniform if $U < 10\%$. Figure 4 shows the dependence of the uniformity factor with different input energies of the main amplifier on pump energy. We can clearly see that the uniformity factor declines with the input energy increases from 0.87 to 4.34 mJ when there is no pump energy of main amplifier. In this condition, the rising amplitude envelope of a burst is maintained for the relatively small gain of the front stage. With the enhancement of pump energy, the uniformity factor generally decreases and then increases. When the leading edge of envelope is amplified to be basically flush with the trailing edge, the uniformity factor reaches the lowest point. Further injecting pump energy leads to the higher leading edge than the trailing edge and the increase of uniformity factor. The higher input energy is injected, the less pump energy is required to achieve the relatively uniform envelope and the

https://doi.org/10.1017/hpl.2023.62 Published online by Cambridge University Press

corresponding output energy is lower. Besides, the similar regular is found in the 6th amplifier. It is not described in this article to avoid repetition. Thus, the uniform envelopes with different output energies can be easily obtained by adjusting pump power of every stage of amplifier without resetting the pre-compensation waveform. Compared with setting pre-compensation envelope achieved by multiple calculations [18, 26, 28], this method is unable to obtain an optimal envelope, but it is more convenient and faster to achieve approximately uniform envelope.

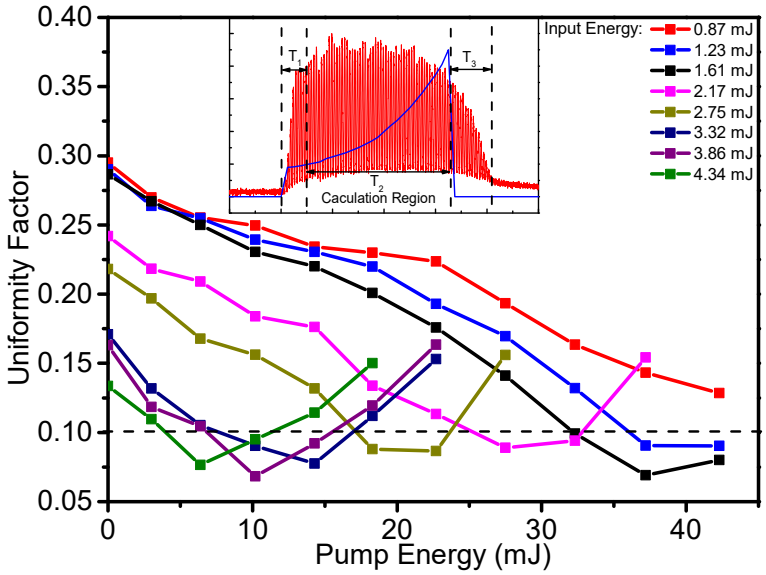

Fig. 4 The envelope uniformity factors with different input energies as a function of main amplifier pump energy; Inset: diagram of calculation region of envelope uniformity factor.

By changing the parameters of AWG-1, the repetition rate and intra-burst duty-cycle can be adjusted conveniently. As shown in Fig. 5, the intra-burst repetition rate is tuned from 0.5 to 10 GHz. The fundamental to harmonic frequency ratios are all over 30 dB. This is the widest tuning range of intra-burst repetition rate for reported burst-mode fiber lasers. Figure 6 compares the output performance under different intra-burst duty cycle of 5%, 10%, 25% and 50% at the same pump energy of main amplifier (42.3 mJ) in detail when the repetition rate is fixed at 1 GHz. The energies and peak powers of different burst-mode pulses is shown in Fig. 6(a). As can be observed,

https://doi.org/10.1017/hpl.2023.62 Published online by Cambridge University Press

with increase of intra-burst duty cycle, the output energy elevates from 9.3 mJ to 13.3 mJ. The extraction efficiency and duty cycle show a positive correlation at the same pump energy. However, the peak power significantly enhances, because the total energy is distributed to the shorter burst duration, leading to the higher peak power. It is remarkable that the highest peak power reaches ~3.6 MW at 5% intra-burst duty cycle, which breaks the peak power record for the GHz burst-mode all-fiber lasers. Figure 6(b) illustrates the detail comparison of intra-burst pulse. The intra-burst pulse widths of the 4 cases are about 0.5 ns, 0.24 ns, 96 ps and 48 ps, respectively. As can be seen in Fig. 6(c), the spectrum broadened with the intra-burst duty cycle reduces. The nonlinear effect is stronger for the smaller intra-burst duty cycle due to the higher peak power. In fact, there is limitation of the intra-burst pulse parameters when using EOM to form the burst. In this work, we employ the EOM with the 10 GHz bandwidth, so 10 GHz and ~48 ps is the highest repetition rate and the narrowest intra-burst pulse duration the laser system can reach, respectively. If we want to achieve the higher repetition rate and the narrower intra-burst pulse duration, the EOM with the higher bandwidth (20 GHz or 40 GHz) should be utilized. Moreover, by re-editing the pre-compensation waveforms of the LD seed driver and AWG-2, an arbitrary envelope shape and tunable burst duration can be achieved.

To test the stability of the laser system, the burst-mode pulse energy is recorded for 60 minutes at the maximum output, as shown in Fig. 7. The corresponding RSD of the energy fluctuation is 1.28%. The beam quality at the output of the laser is measured. The output beam quality factor (M^2) at the maximum output energy (13.3 mJ) is 9.05/8.98 at the x/y direction.

https://doi.org/10.1017/hpl.2023.62 Published online by Cambridge University Press

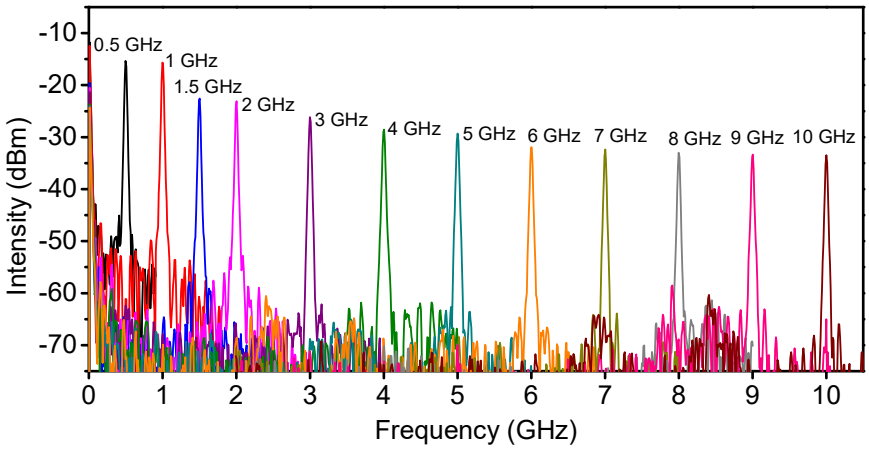

Fig. 5. RF spectrum of different frequency ranging from 0.5 GHz to 10 GHz.

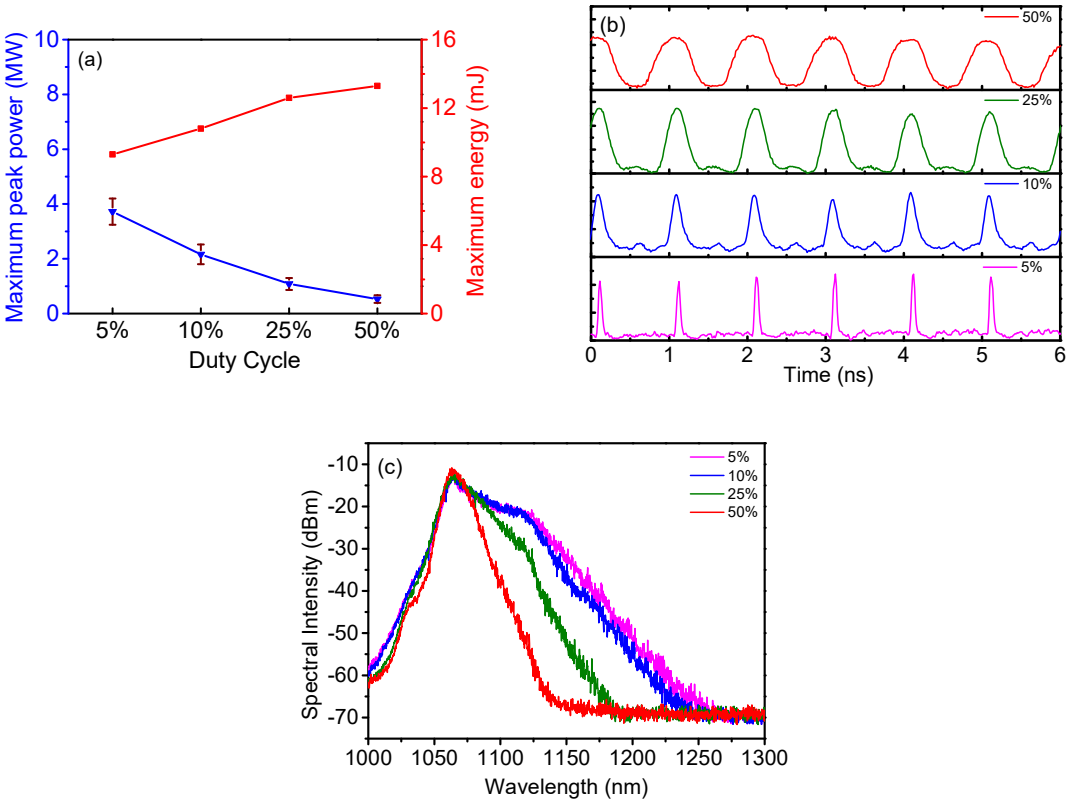

Fig. 6. Performance of the output under different intra-burst duty cycle at the same pump energy (42.3 mJ) when the intra-burst repetition rate is fixed at 1 GHz (a) The energy and peak power; (b)The waveform details of intra-burst pulse; (c) The spectra in 300 nm scanning range.

https://doi.org/10.1017/hpl.2023.62 Published online by Cambridge University Press

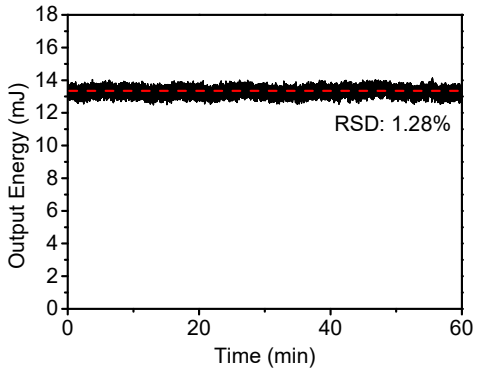

Fig. 7 The long-term stability of energy, measured at an output energy of 13.3 mJ (50 ns, 1 GHz).

IV. Conclusion

In conclusion, we have reported an all-fiber burst-mode laser system operating at a burst repetition rate of 100 Hz. In order to compensate the intense gain saturation effect from the seven stages of fiber amplifier, we propose the double-pre-compensation structure. A uniformly distributed burst-mode pulse with energy of 13.3 mJ and peak power of ~3.6 MW is achieved from a 100 μm core diameter fiber amplifier. The approximately uniform burst envelope can be obtained at different pulse energies by adjusting the pump energy at each stage. Moreover, the repetition rate and pulse duration of the intra-burst pulse can be tuned conveniently for adapting different applications, and the widest reported tuning range (0.5-10 GHz) for intra-burst repetition rate is achieved.

Acknowledgement

This work was supported by the National Natural Science Foundation of China (62205374) and the Research Funds of the State Key Laboratory of Pulsed Power Laser Technology, China (Nos. SKL2021KF07, SKL2020ZR06). The authors are grateful to JinMei Yao, XiaoYong Xu, Sen Guo and WeiDe Hong for their assistance during the experiment.

References

https://doi.org/10.1017/hpl.2023.62 Published online by Cambridge University Press

1. C. Kerse, H. Kalaycıoğlu, P. Elahi, B. Çetin, D. K. Kesim, Ö. Akçaalan, S. Yavaş, M. D. Aşık, B. Öktem, H. Hoogland, R. Holzwarth, and F. Ö. Ilday, "Ablation-cooled material removal with ultrafast bursts of pulses," Nature **537**, 84-88 (2016).
2. S. Kawabata, S. Bai, K. Obata, G. Miyaji, and K. Sugioka, "Two-dimensional laser-induced periodic surface structures formed on crystalline silicon by GHz burst mode femtosecond laser pulses," Int. J. Extrem. Manuf. **5**, 015004 (2023).
3. M. Domke, V. Matylitsky, and S. Stroj, "Surface ablation efficiency and quality of fs lasers in single-pulse mode, fs lasers in burst mode, and ns lasers," Appl. Surf. Sci. **505**, 144594 (2019).
4. K. Mishchik, G. Bonamis, J. Qiao, J. Lopez, E. Audouard, E. Mottay, C. Honninger, and I. Manek-Honninger, "High-efficiency femtosecond ablation of silicon with GHz repetition rate laser source," Opt. Lett. **44**, 2193-2196 (2019).
5. F. Paz-Buclatin, M. Esquivel-González, A. Casasnovas-Melián, O. de Varona, C. Cairós, J. M. Trujillo-Sevilla, K. Kamada, A. Yoshikawa, J. M. Rodríguez-Ramos, and L. L. Martin, "Circularly symmetric nanopores in 3D femtosecond laser nanolithography with burst control and the role of energy dose," Nanophotonics (2023).
6. J. J. Kočica, J. Mur, and J. Petelin, "Laser-based material interactions and ablation processes by bursts of 70 ps pulses," Opt. Express **29**, 22868-22882 (2021).
7. R. S. Marjoribanks, C. Dille, J. E. Schoenly, L. McKinney, A. Mordovanakis, P. Kaifosh, P. Forrester, Z. Qian, A. Covarrubias, and Y. Feng, "Ablation and thermal effects in treatment of hard and soft materials and biotissues using ultrafast-laser pulse-train bursts," Photon. Lasers Med. **1**, 155-169 (2012).
8. P. Elahi, H. Kalaycıoğlu, Ö. Akçaalan, Ç. Şenel, and F. Ö. Ilday, "Burst-mode thulium all-fiber laser delivering femtosecond pulses at a 1 GHz intra-burst repetition rate," Opt. Lett. **42**, 3808-3811 (2017).
9. W. Yue, Y. Zhang, L. Shi, T. Chen, J. Chen, B. Wu, S. Zhang, R. Shu, and Y. Shen, "Porcine skin ablation using mid-infrared picosecond pulse burst," Results Phys. **9**, 100309 (2022).
10. N. Ji, J. C. Magee, and E. Betzig, "Erratum: High-speed, low-photodamage nonlinear imaging using passive pulse splitters," Nat. Methods **6**, 197-202 (2009).

https://doi.org/10.1017/hpl.2023.62 Published online by Cambridge University Press

11. L. Tan, W. Jing, G. I. Petrov, V. V. Yakovlev, and H. F. Zhang, "Photoacoustic generation by multiple picosecond pulse excitation," Med. Phys. **37**, 1518-1521 (2010).
12. O. Volodarsky, Y. Hazan, M. Nagli, and A. Rosenthal, "Burst-mode pulse interferometry for enabling low-noise multi-channel optical detection of ultrasound," Opt. Express **30**, 8959-8973 (2022).
13. X. He, B. Zhang, S. Liu, L. Yang, J. Yao, Q. Wu, Y. Zhao, T. Xun, and J. Hou, "High-power linear-polarization burst-mode all-fibre laser and generation of frequency-adjustable microwave signal," High Power Laser Sci. **9**, e13 (2021).
14. Q. Wu, Y. Zhao, T. Xun, H. Yang, and W. Huang, "Initial Test of Optoelectronic High Power Microwave Generation From 6H-SiC Photoconductive Switch," IEEE Electron Device Lett. **40**, 1167-1170 (2019).
15. J. Zhang, D. Zhang, Y. Fan, J. He, X. Ge, X. Zhang, J. Ju, and T. Xun, "Progress in narrowband high-power microwave sources," Phys. Plasmas **27**, 010501 (2020).
16. X. Chu, J. Liu, T. Xun, L. Wang, H. Yang, J. He, and J. Zhang, "MHz Repetition Frequency, Hundreds Kilowatt, and Sub-Nanosecond Agile Pulse Generation Based on Linear 4H-SiC Photoconductive Semiconductor," IEEE Trans. Electron Devices **69**, 597-603 (2022).
17. J. Petelin, B. Podobnik, and R. Petkovšek, "Burst shaping in a fiber-amplifier chain seeded by a gain-switched laser diode," Appl. Opt. **54**, 4629-4634 (2015).
18. D. N. Schimpf, C. Ruchert, D. Nodop, J. Limpert, A. Tunnermann, and F. Salin, "Compensation of pulse-distortion in saturated laser amplifiers," Opt. Express **16**, 17637-17646 (2008).
19. X. He, B. Zhang, C. Guo, L. Yang, and J. Hou, "4 mJ Rectangular-Envelope GHz-Adjustable Burst-Mode Fiber-Bulk Hybrid Laser and Second-Harmonic Generation," IEEE Photon. J. **13**, 1-9 (2021).
20. H. Kalaycioglu, K. Eken, and F. Ö. Ilday, "Fiber amplification of pulse bursts up to 20 μJ pulse energy at 1 kHz repetition rate," Opt. Lett. **36**, 3383-3385 (2011).
21. H. Yang, Y. Chen, K. Ding, F. Jia, K. Li, and N. Copner, "3.5 ps burst mode pulses based on all-normal dispersion harmonic mode-locked," Appl. Phys. B **126**, 127-135 (2020).
22. C. Kerse, H. Kalaycıoğlu, P. Elahi, Ö. Akçaalan, and F. Ilday, "3.5-GHz intra-burst repetition rate ultrafast Yb-doped fiber laser," Opt. Commun. **366**, 404-409 (2016).

https://doi.org/10.1017/hpl.2023.62 Published online by Cambridge University Press

23. J. Liu, X. Li, S. Zhang, M. Han, and Z. Yang, "Wavelength-Tunable Burst-Mode Pulse With Controllable Pulse Numbers and Pulse Intervals," IEEE J. Sel. Top. Quantum Electron. **25**, 1-5 (2018).
24. T. Bartulevicius, K. Madeikis, L. Veselis, V. Petrauskiene, and A. Michailovas, "Active fiber loop for synthesizing GHz bursts of equidistant ultrashort pulses," Opt. Express **28**, 13059-13067 (2020).
25. T. Chen, H. Liu, W. Kong, and R. Shu, "Burst-mode-operated, sub-nanosecond fiber MOPA system incorporating direct seed-packet shaping," Opt. Express **24**, 20963-20972 (2016).
26. M. Nie, X. Cao, Q. Liu, E. Ji, and X. Fu, "100 μJ pulse energy in burst-mode-operated hybrid fiber-bulk amplifier system with envelope shaping," Opt. Express **25**, 13557-13566 (2017).
27. M. Šajn, J. Petelin, V. Agrež, M. Vidmar, and R. Petkovšek, "DFB diode seeded low repetition rate fiber laser system operating in burst mode," Opt. Laser Technol. **88**, 99-103 (2017).
28. M. Jiang, R. Su, P. Zhang, and P. Zhou, "Arbitrary temporal shape pulsed fiber laser based on SPGD algorithm," Laser Phys. Lett. **15**, 065101 (2018).

https://doi.org/10.1017/hpl.2023.62 Published online by Cambridge University Press